CO_2 sequestration using red gypsum via pH-swing process: Effect of carbonation temperature and NH_4HCO_3 on the process efficiency

Amin Azdarpour[a,*], Mohammad Afkhami Karaei[a], Hossein Hamidi[b], Erfan Mohammadian[c], Maryam Barati[d], Bijan Honarvar[a]

[a] Department of Petroleum Engineering, Marvdasht Branch, Islamic Azad University, Marvdasht, Iran.

[b] School of Engineering, King's College, University of Aberdeen, Aberdeen AB24 3UE, Scotland, UK.

[c] Faculty of Chemical Engineering, Universiti Teknologi MARA, Shah Alam, Selangor, 40100, Malaysia.

[d] Department of Chemical Engineering, Shiraz Branch, Islamic Azad University, Shiraz, Iran.

[*] Corresponding author: A. Azdarpour; amin.azhdarpour@miau.ac.ir; aminazh22@gmail.com

Abstract: The main purpose of this study is to investigate the effect of reaction temperature and NH_4HCO_3 on the overall performance of a pH swing mineral carbonation. The overall performance of the pH swing process is investigated in terms of carbonation efficiency and product purity. Initially, 2 M H_2SO_4 is used for red gypsum dissolution at 70 °C. Then in the second stage, NH_4OH is added for increasing the solution pH and removing the impurities from solutions. Finally, CO_3^{2-} is introduced to calcium rich solution in the form of pure CO_2 and NH_4HCO_3. The experimental results show that using NH_4HCO_3 improves carbonation efficiency and product purity.

Carbonation efficiency attains a maximum value at 75 °C and then decreases gradually with increasing temperature up to 300 °C, with both CO_2 and NH_4HCO_3. In this research, $CaCO_3$ with the maximum purity of 99.05% is produced successfully when NH_4HCO_3 is used as a CO_3^{2-} source.

***Keywords*: CO_2 sequestration, Carbon capture and storage, Mineral carbonation, Calcium carbonate, pH swing.**

1. Introduction

Global warming and the consequent change of climate are the main environmental concerns in the 21st century. Huge amounts of greenhouse gases, and in particular CO_2, are released into the atmosphere from an over dependency on fossil fuels as a main energy source and other large industries such as cement manufacture. [1-4]. Increasing atmospheric CO_2 level concentration to about 400 ppm in 2015 is the result of this over dependency to fossil fuels, which has created an emergency situation from an environmental point of view [1,4,5-8].

Carbon capture and storage (CCS) consists of the separation of CO_2 from gaseous waste streams, the transport of CO_2 to storage locations and finally long-term storage of CO_2 from the atmosphere [4]. CO_2 injection into geological formation, saline aquifers and ex-situ mineral carbonation are some of the studied CO_2 storage techniques [9-11]. Most of these methods can be applied to large CO_2 emitters and their high CO_2 capture efficiency make CCS techniques very attractive to mitigate CO_2 emissions. Although it is true that those methods have high CO_2 capture efficiency, their costs, applicability in

term of CO_2 separation/origin as well as social acceptability, have limited their attractiveness for the companies. In addition, CCS techniques are known as the long-term technology to reduce the negative impacts of high CO_2 concentration on the earth eco-system, however, switching to non-fossil fuels and green technologies are vital as well [1,4, 11-15].

Mineral carbonation, the reaction of metal ions such as calcium, magnesium and iron with CO_2 to produce solid carbonates was first introduced by Seifritz in 1990 [16]. The key point of using this approach is that the produced carbonates are permanently solid and stable whereby there is no risk of CO_2 leakage. The energy state of carbonates are 160-180 kJ/mol lower than the energy state of CO_2, which makes the produced carbonates very stable. In addition, due to availability of feedstock (both natural minerals and industrial wastes) billions of tonnes of CO_2 could be sequestered through mineral carbonation. However, technical challenges to increase carbonation rate and decrease energy penalty and operating cost still exist [4,13,14,16,17].

Red gypsum has received significant attention recently to sequester CO_2. Availability of significant amounts of calcium and iron gives red gypsum unique properties to be used as the raw material for mineral carbonation. Red gypsum is a byproduct produced during a stepwise process for extracting titanium dioxide (TiO_2) from ilmenite [14,18-20]. Since the introduction of mineral carbonation, different approaches have been tested in the literature. Some have used direct methods [21-25] and some have used indirect methods [14,26-29]. Reaction temperature, CO_2 pressure, reaction time, nature of feedstocks, reactor configuration, carbonation route, and the type of solvent are important factors that can affect the overall efficiency of the mineral

carbonation process [4,13,14]. In general, carbonation efficiency is usually low through direct methods, however, they sound more viable from a cost and energy analysis points of view. On the other hand, higher conversion rates as well as higher product purity make indirect processes more attractive than direct methods [4,13].

In this study, the effect of reaction temperature (25-300 ºC) on the overall efficiency of red gypsum carbonation through a pH swing process is investigated. The aim of this study is to understand the impact of reaction temperature on the carbonation efficiency, removal efficiency and carbonates purity. Pure CO_2 and NH_4HCO_3 are added to the calcium rich solutions. This idea provides a novel idea of using two different CO_3^{2-} source to precipitate carbonates from red gypsum through a pH swing process.

2. Materials and methods

Initially, H_2SO_4 is used to extract calcium ions from red gypsum, followed by NH_4OH addition to remove impurities in the second stage. Finally, carbonates are precipitated out of solution using CO_2 and NH_4HCO_3. Final products are characterized using X-ray diffraction (XRD), thermal gravimetric analysis (TGA), and field emission scanning electron microscope (FESEM) to determine carbonation efficiency and carbonates purity.

2.1 Materials

Red gypsum samples were taken from landfills of red gypsum in Kemaman, Terengganu, Malaysia. After sample collection, hydrated samples were dried in an oven at 45 °C. The chemicals (NH_4OH, H_2SO_4, and NH_4HCO_3) used in this study were purchased from Rankem and the CO_2 tanks with purity of more than 99% were purchased from Malaysian Oxygen. The chemical composition of red gypsum was analyzed using

XRF and the results are shown in Table 1. As the results show, red gypsum mainly consists of CaO and Fe_2O_3 along with some other minor compounds, which makes it a very attractive feedstock for mineral carbonation purposes.

Table 1. Chemical content of red gypsum from XRF

Compound	Concentration (wt%)
CaO	32.20
SO_3	31.60
Fe_2O_3	28.99
TiO_2	5.64
SiO_2	1.90
Al_2O_3	0.39
MnO	0.41
RuO_2	0.39
Eu_2O_3	0.26
V_2O_5	0.22
ZrO_2	0.06
CuO	0.06
HgO	0.03
Cr_2O_3	0.03
ZnO	0.04
SrO	0.03

2.2 Experimental methods

The pH swing experiments consist of three main steps as illustrated in Fig. 1. The first step was to extract iron and calcium ions from the red gypsum using H_2SO_4. The second step was to remove impurities (mainly iron) from the solutions by adding NH_4OH. Finally, CO_3^{2-} was added in two different ways to the calcium rich solutions to precipitate $CaCO_3$. One method was to introduce pure CO_2 from a CO_2 tank and the other method was by NH_4HCO_3 addition.

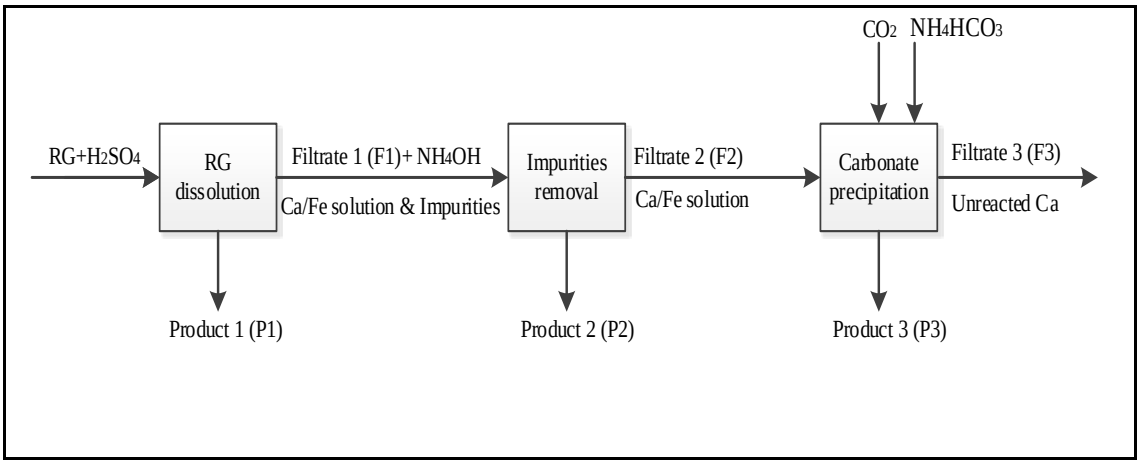

Fig. 1: Overall pH swing carbonation process.

2.2.1 Dissolution and carbonation of red gypsum

A three-necked glass reactor with 500 mL capacity is used for dissolution experiments as shown in Fig. 1(a) of our previously published article [14]. A mechanical stirrer is used for mixing all solutions and a heating mantle is used to control the reaction temperature. In addition, a water cooled condenser is used to prevent solution vapor from escaping. The carbonation experiments are conducted in a 100 mL (made of stainless steel 316) high pressure and temperature (HPHT) autoclave reactor, as shown in Fig. 1(b) of our previously published article [14]. The autoclave reactor can withstand the maximum operating temperature of 450 °C and CO_2 pressure of 200 bar. The temperature of furnace is controlled using a temperature controller and CO_2 gas is deliver to the reactor through a 1/8 inch stainless steel tubing.

Three sets of dissolution experiments are performed in general. Two sets are used for carbonate precipitation with CO_2 and the last set is used for carbonate precipitation with NH_4HCO_3. Initially, 200 mL of 2M H_2SO_4 is prepared and poured into the reactor. Then the reaction temperature is adjusted and fixed at 70 °C using a temperature

controller. Then, a batch of 10 g of red gypsum, with the average particle size of 100-212 μm, is added to the solution. Immediately after the red gypsum is added, the solution is stirred at 1000 rpm for 60 min. After stopping the reaction, solutions are filtered immediately. After filtration, the solution is named as filtrate 1 (F1) and the solid is named as product 1 (P1). The concentration of iron and calcium in the solutions is measured using inductively coupled plasma optical emission spectrometry (ICP-OES). Equations (1) and (2) are used to calculate the extraction efficiency of calcium and iron after red gypsum dissolution. In these equations, the $M_{Ca\text{-}extracted}$ and $M_{Fe\text{-}extracted}$ is the mass (g) of the calcium and iron in the leachate obtained after the extraction experiments. The M_t is the total mass (g) of the RG used in the extraction test, which is 10 g. The C_{CaO} and C_{Fe2O3} are the calcium oxide and iron oxide content of the red gypsum. The Mw is the molecular weight of Ca, CaO, Fe, Fe_2O_3, and CO_2 (g/mol).

$$\text{Ca extraction efficiency (\%)} = \frac{M_{Ca\text{-}extracted}\ (g),\ (F1)}{M_t\ (g) \times \frac{C_{CaO}\ (\%)}{100} \times \frac{Mw_{Ca}\ (g/mol)}{Mw_{CaO}\ (g/mol)}} \times 100 \quad (1)$$

$$\text{Fe extraction efficiency (\%)} = \frac{M_{Fe\text{-}extracted}\ (g),\ (F1)}{M_t (g) \times \frac{C_{Fe_2O_3}\ (\%)}{100} \times \frac{Mw_{Fe}\ (g/mol)}{Mw_{Fe_2O_3}\ (g/mol)}} \times 100 \quad (2)$$

The second step of the pH swing process is to remove impurities from the solutions by NH_4OH addition. Initially, 100 mL of F1 sample is removed from the reactor and poured into a beaker. Then NH_4OH is added to the solution slowly, one drop at a time, to increase the solution pH, whilst measuring the solution pH all the time with a pH

meter. The addition of NH_4OH to solutions is continued until the desired pH of around 9.5 is reached. Then, NH_4OH addition is stopped and solutions filtered accordingly. After filtration, the solution is named as filtrate 2 (F2) and solid residues are named as product 2 (P2). Finally, ICP-OES is used to measure the concentrations of calcium and iron in F2 solutions.

The third step of the pH swing process is carbonate precipitation. In this step, 50 mL of calcium rich solution is poured into the reactor. Then, the reactor is sealed air tight and pressurized by injecting CO_2 at the desired pressure (1 and 8 bar). The reactor is heated to the desired temperature (25 to 300 °C). Each carbonation reaction lasts 30 minutes. After depressurizing the reactor each solution is filtered. After this step, solutions are named as filtrate 3 (F3) and solid samples named as product 3 (P3). In order to use NH_4HCO_3 as the CO_3^{2-} source, pure solid NH_4HCO_3 is added into the calcium rich solution. After adding NH_4HCO_3 to the calcium leachate, the reaction lasts 30 minutes.

The concentrations of calcium and iron are used to calculate iron and calcium removal efficiency. Equation (3) represents the calcium removal efficiency, where in this equation $M_{Ca\text{-}extracted}$ is the mass of calcium in stage two (F2 solutions) and $M_{Ca\text{-}carbonated}$ is the mass of calcium after carbonation experiments. On the other hand, Equation (4) represents the iron removal efficiency.

$$\text{Ca removal efficiency (\%)} = \frac{M_{\text{Ca-extracted (g)}}, (F2) - M_{\text{Ca-carbonated (g)}}, (F3)}{M_{\text{Ca-extracted (g)}}, (F2)} \times 100 \quad (3)$$

$$\text{Fe removal efficiency (\%)} = \frac{M_{\text{Fe-extracted (g)}}, (F2) - M_{\text{Fe-carbonated (g)}}, (F3)}{M_{\text{Fe-extracted (g),}} (F2)} \times 100 \quad (4)$$

Calcium carbonation efficiency is calculated using Equation (5), where $M_{Ca\text{-}carbonated}$ represents the mass of calcium after carbonation experiments (F3 samples) and $M_{Ca\text{-}extracted}$ represents the mass of calcium after extraction experiments (F1 samples). On the other hand, Equation (6) is used to determine iron carbonation efficiency. The M_t in these equation represents the total mass of red gypsum in grams used in extraction experiments. The $C_{CaO\ and}\ C_{Fe2O3}$ represents the calcium and iron oxide content present in red gypsum. In addition, the molecular weights of calcium and iron, as well as their oxides forms, are also shown in these equations.

$$\text{Ca carbonation efficiency}(\%)=\frac{M_{\text{Ca-extracted (g)}},(\text{F1})-M_{\text{Ca-carbonated (g)}},(\text{F3})}{M_t(\text{g})\times\frac{C_{CaO}(\%)}{100}\times\frac{MW_{Ca}(\text{g/mol})}{MW_{CaO}(\text{g/mol})}}\times 100 \quad (5)$$

$$\text{Fe carbonation efficiency}(\%)=\frac{M_{\text{Fe-extracted (g)}},(\text{F1})-M_{\text{Fe-carbonated (g)}},(\text{F3})}{M_t(\text{g})\times\frac{C_{Fe_2O_3}(\%)}{100}\times\frac{MW_{Fe}(\text{g/mol})}{MW_{Fe_2O_3}(\text{g/mol})}}\times 100 \quad (6)$$

2.2.2 Characterization of products

The final products are analyzed with FESEM, XRD, and TGA. The composition and morphology of the products are analyzed using a FESEM JEOL JSM-6400 with 20 kV beam voltage and 15 mm working distance. 1000 mg of each sample coated with gold at 2.2 kV for 90 s is used for each analysis. A Philips analytical XRD machine with the scanning speed of 1 degree per minute from 5° to 70° under 40 kV/40 mA is used for XRD analysis. In addition, TGA is performed using a thermal TGA Q500, TA Instrument for purity calculations. Initially, 20 mg of each sample is heated from ambient temperature to 1000 °C under nitrogen atmosphere at 10 °C/min. The purity of both

calcium carbonate ($CaCO_3$) and iron carbonate ($FeCO_3$) is also examined, because of the availability of both calcium and iron in the solutions. In this study, $CaCO_3$ purity is defined as the percentage of $CaCO_3$ in the final product. The purity of $CaCO_3$ and $FeCO_3$ is calculated using Equations (7) and (8), respectively. In these equations, *P* stands for product purity, ΔW represents the weight loss of the sample from TGA and molecular weight is shown by MW. The weight loss of $FeCO_3$ occurs at 200-450 °C, and weight loss of $CaCO_3$ occurs at 600-850 °C due to CO_2 evaporation.

$$P_{CaCO_3} = \frac{\Delta W(\%) \times Mw_{CaCO_3}}{Mw_{CO_2}} \times 100 \quad (7)$$

$$P_{FeCO_3} = \frac{\Delta W(\%) \times Mw_{FeCO_3}}{Mw_{CO_2}} \times 100 \quad (8)$$

3. Results and Discussions

3.1 Calcium solution preparation and pH regulation

Table 2 represents the concentrations of calcium and iron ions during the dissolution of red gypsum and pH adjustment steps. Initially, 2 M H_2SO_4 is used to extract calcium and iron from raw red gypsum. The ICP-OES results show that all calcium ions are extracted with 2 M H_2SO_4, which results in 100% calcium extraction efficiency from red gypsum in all experiments. On the other hand, the concentration of extracted iron from red gypsum is in the range of 2912-3510 mg/L, which results in an extraction efficiency of 57-69%.

In the second step of the pH swing process, NH_4OH is added to the solutions for removing the impurities from calcium rich solutions. The solution pH after NH_4OH addition to solutions are between 9.4 to 9.5. The ICP-OES results show that after pH adjustment, a significant amount of iron ions are separated from solutions and only a small amount of calcium ion is precipitated. The concentration of calcium ions in the filtrate 2 solutions are in the range of 11362-11388 mg/L and the concentration of iron ions are in the range of 148-280 mg/L, respectively. The NH_4OH addition to filtrate 1 samples results in an average iron separation of 94% from the solutions.

Table 2: Concentrations of calcium and iron during the first and second stage of the pH swing process

Set	Filtrate 1 (mg/L)		Filtrate 2 (mg/L)	
	Calcium	**Iron**	**Calcium**	**Iron**
1	*11509*	*2912*	*11388*	*233*
	11509	*3409*	*11373*	*205*
	11509	*3115*	*11370*	*249*
	11509	*3510*	*11365*	*211*
	11509	*3333*	*11362*	*167*
	11509	*3358*	*11377*	*269*
	11509	*3459*	*11380*	*173*
2	11509	2912	11371	269
	11509	3409	11373	173
	11509	3115	11370	148
	11509	3510	11365	167
	11509	3333	11364	233
	11509	3358	11377	205
	11509	3459	11380	249
3	*11509*	*3345*	*11383*	*148*
	11509	*3502*	*11362*	*182*
	11509	*3018*	*11369*	*214*

	11509	*2999*	*11371*	*202*
	11509	*3257*	*11374*	*280*
	11509	*3108*	*11387*	*259*
	11509	3391	11381	208
The reaction condition of each sample is shown in Table 3.				

3.2 Carbonation and removal efficiency

Carbonation efficiency of pH swing experiments is calculated by considering the concentration of calcium and iron in filtrate 1 and filtrate 3. On the other hand, removal efficiency is determined using the values of calcium and iron in filtrate 2 and filtrate 3. The reaction temperature increases from 25 to 300 °C at a constant reaction time of 30 minutes. CO_2 with constant pressure of 1 and 8 bar is injected into the reactor. Another set of experiments is carried out using NH_4HCO_3 as the CO_3^{2-} source at atmospheric pressure. Finally, carbonation efficiency was determined for each experiments. Table 3 represents the summary of calculated carbonation and removal efficiency, as well as the concentrations of iron and calcium after the carbonation experiments.

Table 3: Detailed carbonation conditions and efficiencies

Set	**Concentrations after carbonation, F3 (mg/L)**		**Carbonation conditions**				**Efficiencies**		
	Calcium	**Iron**	**Temperature (°C)**	**Pressure (bar)**	**Reaction time (min)**	**CO_3^{2-} source**	**Calcium carbonation efficiency (%)**	**Calcium removal efficiency (%)**	**$CaCO_3$ purity (%)**
1	*7562*	*<DL*	*25*	*1*	*30*	*CO_2*	*34*	*34*	*91.28*
	6580	*<DL*	*50*	*1*	*30*	*CO_2*	*43*	*42*	*91.98*
	5430	*<DL*	*75*	*1*	*30*	*CO_2*	*53*	*52*	*89.99*
	5978	*<DL*	*100*	*1*	*30*	*CO_2*	*48*	*47*	*91.67*
	6987	*<DL*	*150*	*1*	*30*	*CO_2*	*39*	*39*	*92.57*
	8053	*<DL*	*200*	*1*	*30*	*CO_2*	*30*	*29*	*89.85*

	9435	*<DL*	*300*	*1*	*30*	*CO_2*	*18*	*17*	*92.16*
2	1859	<DL	25	8	30	CO_2	85	84	91.31
	1685	<DL	50	8	30	CO_2	86	85	92.21
	1786	<DL	75	8	30	CO_2	86	85	94.57
	1863	<DL	100	8	30	CO_2	85	84	93.72
	1957	<DL	150	8	30	CO_2	84	83	91.64
	2257	<DL	200	8	30	CO_2	81	80	92.01
	2483	<DL	300	8	30	CO_2	79	78	91.39
3	*2749*	*<DL*	*25*	*1*	*30*	*NH_4HCO_3*	*76*	*76*	*99.05*
	920	*<DL*	*50*	*1*	*30*	*NH_4HCO_3*	*92*	*92*	*98.74*
	218	*<DL*	*75*	*1*	*30*	*NH_4HCO_3*	*98*	*98*	*96.02*
	843	*<DL*	*100*	*1*	*30*	*NH_4HCO_3*	*93*	*93*	*97.57*
	1394	*<DL*	*150*	*1*	*30*	*NH_4HCO_3*	*88*	*88*	*95.12*
	1693	*<DL*	*200*	*1*	*30*	*NH_4HCO_3*	*85*	*85*	*95.58*
	2001	*<DL*	*300*	*1*	*30*	*NH_4HCO_3*	*83*	*82*	*96.49*

3.2.1 Carbonation by CO_2

The pH swing experimental results show that reaction temperature affects carbonation efficiency significantly. The minimum calcium carbonation efficiency is at 25 °C and it increased to its maximum value at a temperature of 75 °C. On the other hand, calcium carbonation efficiency reduces with a further increase of the reaction temperature to 300 °C. Under 1 bar CO_2 pressure, a carbonation efficiency of 34%, 53%, and 18% is achieved under 25, 75 and 300 °C, respectively. However, carbonation efficiency increases significantly with increasing CO_2 pressure to 8 bar. Carbonation efficiency of 85%, 86% and 79% is achieved under reaction temperatures of 25, 75, and 300 °C, respectively.

Similarly, calcium removal efficiency exhibits the same behavior as carbonation efficiency. Initially, calcium removal efficiency increases with increasing the reaction temperature up to 75 °C, and further increasing the temperature to about 300 °C decreases removal efficiency. A calcium removal efficiency of 34%, 52%, and 17% is achieved under 25, 75 and 300 °C, respectively when CO_2 pressure of 1 bar is used. The

calcium removal efficiency is enhanced substantially with increasing the CO_2 pressure to 8 bar. In this case, a calcium removal efficiency of 84%, 85% and 78% is achieved under 25, 75 and 300 °C, respectively.

On the other hand, iron removal efficiency exhibited different behavior, as it resulted in 100% removal efficiency in all experiments. Due to the low concentration of iron ions before the carbonation stage (iron concentration in F2 solutions), all iron ions reacted with CO_2, which results in the complete reaction of iron ions during experiments.

The results achieved in this study are comparable with the literature data. Santos et al. [30] investigated the carbonation efficiency of continuous casting (CC) slags with respect to changes of reaction temperature. Their experiments showed that carbonation efficiency reached a maximum level at 90 °C and then decreased with increasing temperature up to 180 °C. In addition, they concluded that CO_2 solubility is more significantly affected by temperature at lower pressures than at higher pressures. Sun et al. [31] also concluded that carbonate production from steelmaking slag with NH_4Cl as the leaching solution reaches a maximum value at 60 °C reaction temperature. In addition, further increasing the reaction temperature, deceased precipitation, which is due to the decrease in CO_2 solubility. In another study by Zhang et al [32], magnesium conversion to $MgCO_3$ showed similar behavior with increasing temperature, as the maximum magnesium conversion to MgCO3 occurred at 100 °C.

CO_2 solubility and carbonic acid dissociation are temperature dependent, which can directly affect carbonation efficiency. Increasing reaction temperature decreases CO_2 solubility, which creates an unfavorable condition for CO_2 sequestration. On the other hand, increasing CO_3^{2-} activity favors carbonate precipitation. CO_3^{2-} activity exhibits

different behavior with increasing temperature. CO_3^{2-} activity reaches a maximum level and then starts decreasing with further increases in the reaction temperature. There is always a balance between carbonic acid dissociation and CO_2 solubility with increasing temperature. Therefore, carbonation efficiency attains a maximum level with increasing temperature to some extent [32]. On the other hand, Henry's law constant for CO_2, K_H, the first and the second dissociation constants, Ka_1 and Ka_2, for H_2CO_3 can be used to explain effect of CO_2 pressure on carbonation efficiency. Equations (9) to (11) show CO_2 dissolution, first and second dissociation of carbonic acid and their constants, respectively, while the concentration of CO_3^{2-} is shown in Equation (12). At constant temperature, K_H, Ka_1 and Ka_2 are constant and the concentration of CO_3^{2-} is only affected by CO_2 pressure and pH [33]. Thus, concentration of CO_3^{2-} can be simply increased by increasing CO_2 pressure as solution pH is constant in this study. This is the reason for having higher carbonation efficiencies when 8 bar CO_2 pressure is used rather than 1 bar CO_2 pressure, in this study.

$$CO_2\,(g) + H_2O \leftrightarrow H_2CO_3^* \qquad [H_2CO_3^*]=K_H.P_{CO2} \qquad (9)$$

$$H_2CO_3^* \leftrightarrow H^+ + HCO_3^- \qquad K_{a1}=\frac{[H^+][HCO_3^-]}{[H_2CO_3^*]} \qquad (10)$$

$$HCO_3^- \leftrightarrow H_+ + CO_3^{2-} \qquad K_{a2}=\frac{[H^+][CO_3^{2-}]}{[HCO_3^-]} \qquad (11)$$

$$[CO_3^{2-}]=\frac{K_{a1}.K_{a2}.K_H P_{CO2}}{[H^+]^2} \qquad (12)$$

3.2.2 Carbonation by NH_4HCO_3

Carbonate precipitation is mainly controlled by the reaction between calcium ions and CO_3^{2-} in which the higher the concentrations of these ions the higher the chances of carbonates precipitation. The concentration of calcium ions available in the solution is nearly constant in all our experiments, thus, increasing the concentration of CO_3^{2-} could provide further enhancements in carbonation efficiency. An advantage of using NH_4HCO_3 over pure CO_2 is that NH_4HCO_3 is a better source of CO_3^{2-}. Hence, a set of carbonation experiments are conducted and carbonation and removal efficiencies are determined accordingly. Table 3 shows a carbonation efficiency of 76% under ambient temperature and an increase to its maximum value of 98% when the reaction temperature is 75 °C. Further increasing the temperature to about 300 °C results in a carbonation efficiency of 83%. On the other hand, calcium removal efficiency also shows similar behavior as carbonation efficiency. A calcium removal efficiency of 76, 98, and 82% is achieved under 25, 75 and 300 °C, respectively.

Another observation from the experimental results is that carbonation efficiency is much higher when NH_4HCO_3 is used as CO_3^{2-} source rather than CO_2. Fig. 2 represents the carbonation efficiency under 1 and 8 bar CO_2 pressure as well as NH_4HCO_3 utilization at atmospheric pressure. Carbonation efficiency is about 18-53% with 1 bar CO_2 pressure while it increases to about 79-86% under 8 bar CO_2 pressure and finally, it increases to about 76-98% when NH_4HCO_3 provides CO_3^{2-}. The reason behind this is that theoretically, NH_4HCO_3 provides a better source of CO_3^{2-} than CO_2. In the case of NH_4HCO_3, 1 mol of CO_3^{2-} is produced by the reaction of 1 mol of NH_3 and 1 mol of NH_4HCO_3, which produces 1 mol of $(NH_4)_2CO_3$ and subsequently 1 mol of CO_3^{2-}. On the

other hand, to produce 1 mol of CO_3^{2-} from CO_2, 2 mol of NH_3 and 1 mol of CO_2 are required. Thus, more CO_3^{2-} will be formed when NH_4HCO_3 is used as CO_3^{2-} source rather than CO_2. In addition, NH_4HCO_3 dissociates in one single step to form CO_3^{2-}, while it takes two steps from the H_2CO_3 to dissociates and form CO_3^{2-}. Thus, the amount of CO_3^{2-} provided by NH_4HCO_3 hydrolysis is several magnitudes higher than that by H_2CO_3 dissociation. These results are comparable with the results of the experiments conducted by He et al. [34].

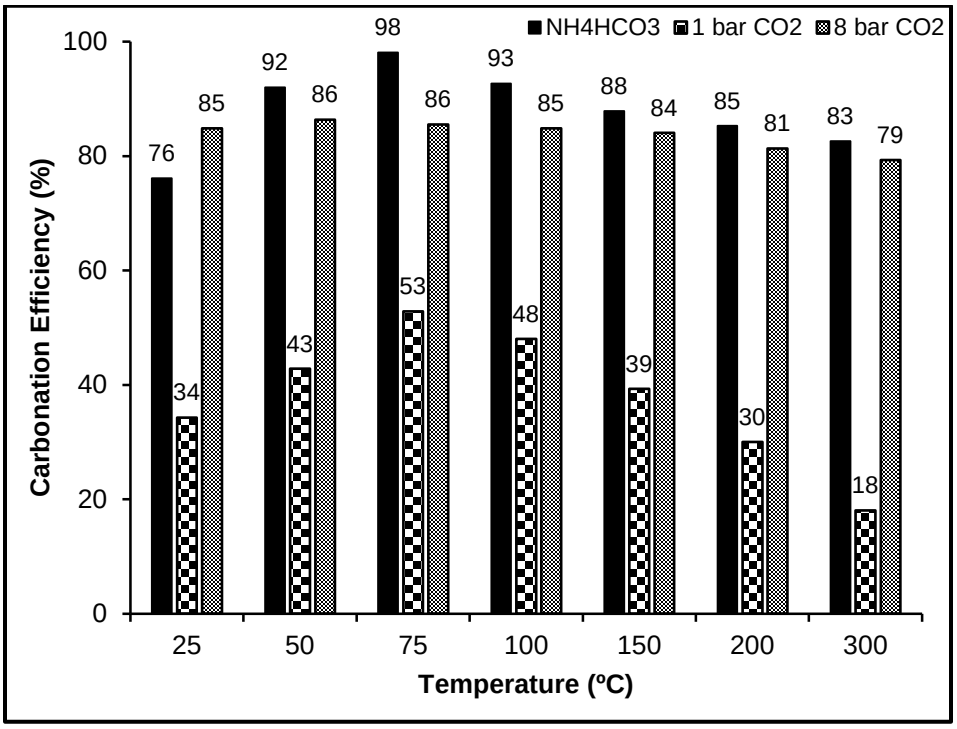

Fig. 2: Carbonation efficiency versus temperature using NH_4HCO_3 and CO_2 (1 and 8 bar).

3.3 Characterization of carbonates

TGA results are used to determine the purity of carbonates. Both calcium and iron ions are successfully reacted with CO_2 and both $CaCO_3$ and $FeCO_3$ precipitated in the final product. However, $CaCO_3$ purity is expected to be higher than the $FeCO_3$, because the concentration of reacted calcium is higher than iron. The $CaCO_3$ purity, as the main focus of this research, is in the range of 89.85% to 94.57% when CO_2 is used. On the other hand, $CaCO_3$ purity increases to between 95.12 and 99.05% when NH_4HCO_3 is added to the leachates. Table 3 presents the purity of $CaCO_3$ when NH_4HCO_3 and CO_2 are used.

$CaCO_3$ purity is found to be related to the concentration of reacted iron ions during the reaction. The higher the concentration of reacted iron, the lower the $CaCO_3$ purity. Fig. 3 represents the relationship between $CaCO_3$ purity and the concentration of reacted iron ions during all carbonation experiments. As shown in this figure, $CaCO_3$ purity has an inverse relationship with the concentration of reacted iron. Both calcium and iron ions easily react with CO_3^{2-} to form $CaCO_3$ and $FeCO_3$. The main objective of this research is to produce high purity $CaCO_3$. Thus, complete separation of impurities and in particular iron ions from solutions prior to the carbonation stage provides a platform for ideal reaction of calcium ions with CO_3^{2-}. Unfortunately, complete separation of impurities is not successful in this study and about 148 to 280 mg/L of iron ions are present in the solution prior to carbonation. However, these low concentrations of iron ions react with CO_3^{2-} and result in a $CaCO_3$ purity of slightly lower than the expected value.

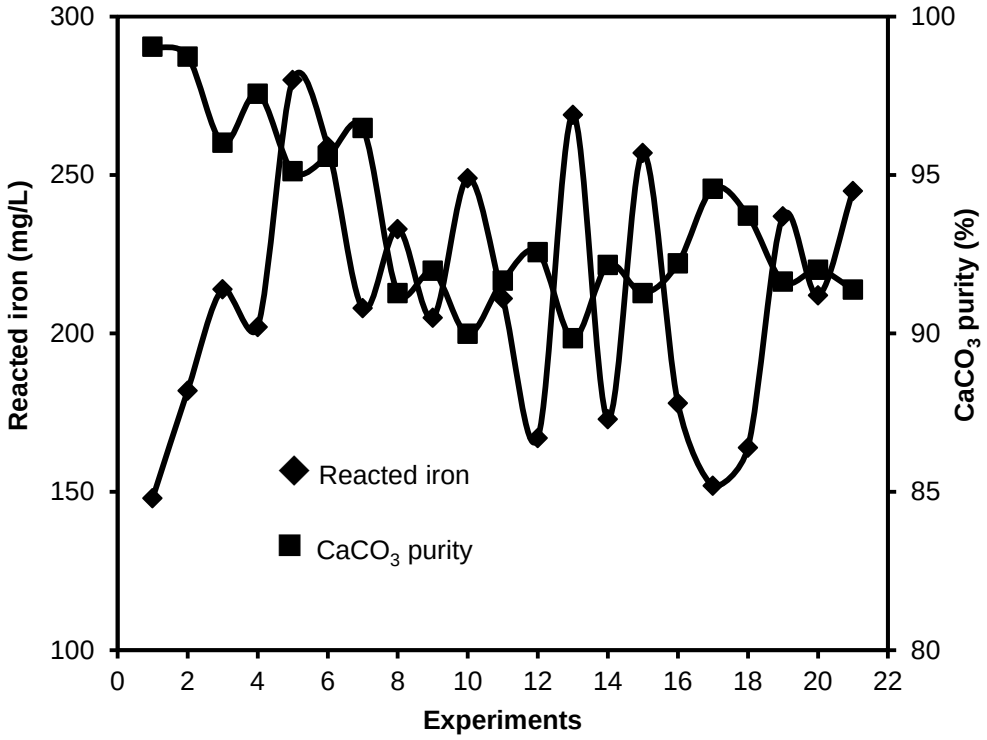

Fig. 3: $CaCO_3$ purity and concentration of reacted iron.

It is stated in the literature that the most common structure of vaterite is spherical, calcite is rhombohedral and aragonite is needle shaped [14,35]. Fig. 4 represents the FESEM analysis of the carbonation products when CO_2 and NH_4HCO_3 are used. Fig. 4(a-d) represents the carbonation products under CO_2 utilization. As shown in these figures, calcite, vaterite and aragonite are the main products of the carbonation reactions, however traces of $FeCO_3$ are clearly shown in these figures as well. On the other hand, Fig. 4(e, f) represents the carbonation products when NH_4HCO_3 is used. As shown in these figures, calcite is the major component of the carbonation product. Perfectly rhombohedral structures of calcite are shown in these pictures with magnifications of 1 µm and 200 nm. The FESEM analysis of carbonation products clearly show that calcites are the main

polymorphs of $CaCO_3$. A perfectly rhombohedral structure of final product confirms the high purity of $CaCO_3$ as the main product of the carbonation experiments, as expected.

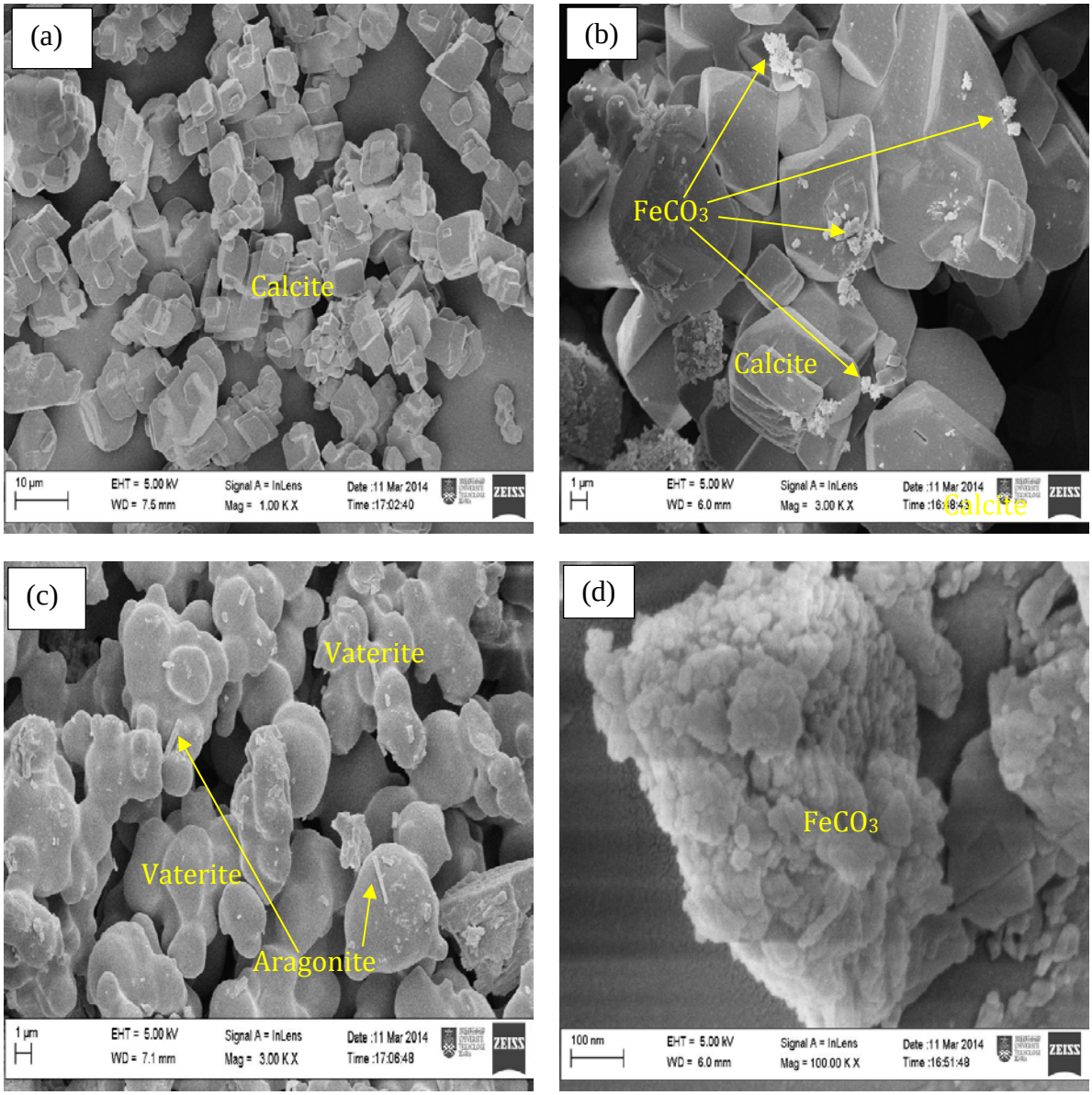

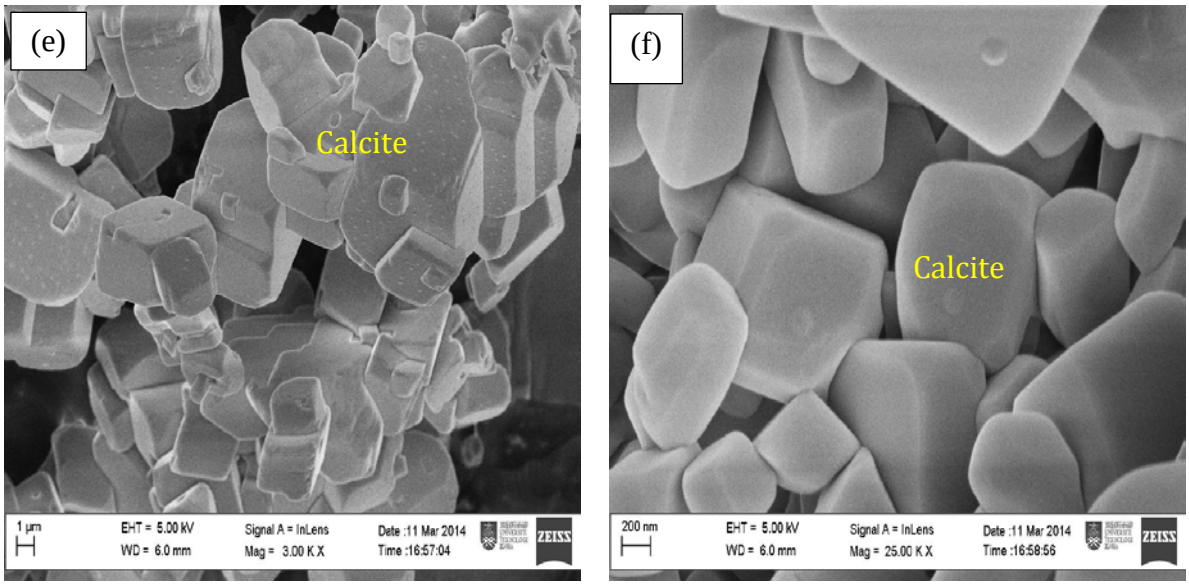

Fig. 4: FESEM analysis of carbonate products.

Fig. 5 shows the XRD pattern of carbonation products at temperatures of 75 °C (spectra a), 150 °C (spectra b) and 200 °C (spectra c). Spectra (a) shows that the representative peaks of A, C, V, and S are detected, which are assigned to aragonite, calcite, vaterite and siderite, respectively. In spectra (b), which is the carbonation product at 150 °C, the representative peaks of calcite, vaterite and siderite are detected, which clearly prove the success of the carbonation experiments. Finally, in spectra (c), the representative peaks of vaterite and siderite are detected, which clearly prove that only vaterite can be formed at temperatures of above 170 °C. It is stated in the literature that vaterite, calcite and aragonite could be produced under 80 °C, while at temperatures of about 170 °C vaterite and calcite are produced. Also, only vaterite is produced when the reaction temperature is above 170 °C [14,35,36].

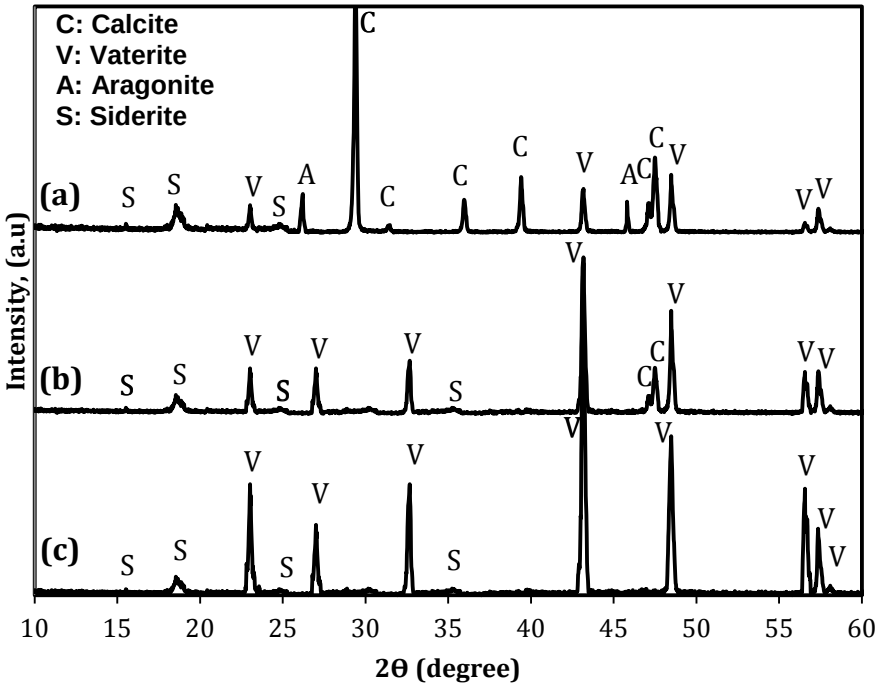

Fig. 5: XRD pattern of (a) carbonation product at 75 °C, (b) carbonation product at 150 °C and (c) carbonation product at 200 °C.

The main weight loss of $FeCO_3$ occurs between 200-450 °C and the main weight loss of $CaCO_3$ occurs between 600-850 °C. These weight losses are due to the evolution of CO_2 from decomposition of carbonates [14]. Fig. 6 represents the TGA and DTA curves of the carbonation product under CO_2 and NH_4HCO_3 utilization. The figure shows that a minor weight loss occurs between 200-450 °C, which represents the presence of $FeCO_3$ in the final product. $FeCO_3$ purity is higher when CO_2 is used rather than NH_4HCO_3, thus this weight loss is more sever when CO_2 is used. In addition, a major weight loss occurs between 600-850 °C, which is due to the evolution of CO_2 from $CaCO_3$. $CaCO_3$ purity is much higher when NH_4HCO_3 is used, thus this weight loss is more sever for the TGA curve of carbonation product with NH_4HCO_3, compared with

CO_2. These curves are perfect indications of the presence of $CaCO_3$ and $FeCO_3$ in the final products.

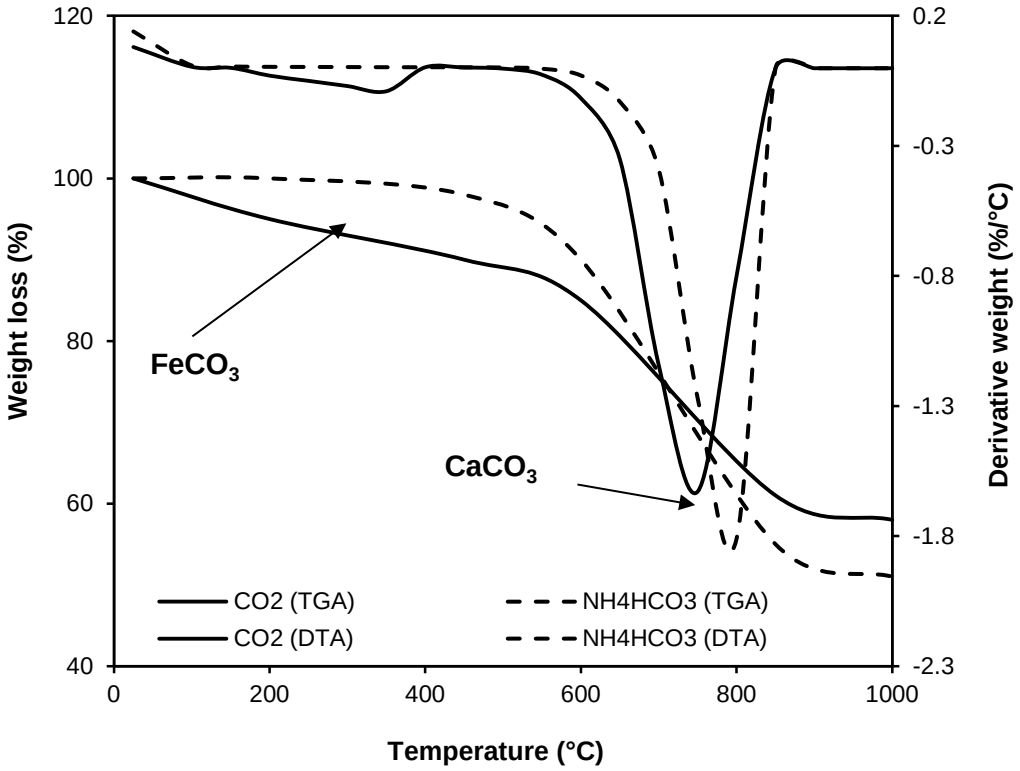

Fig. 6: TGA curves of carbonation products using NH_4HCO_3 and CO_2.

4. Conclusions

This study investigated the effect of different reaction temperatures on the overall efficiency of mineral carbonation of red gypsum using CO_2 and NH_4HCO_3 as the CO_3^{2-} source. The following conclusions are drawn from the experiments performed:

1. In general, the experiments conducted using NH_4HCO_3 showed better results in terms of $CaCO_3$ purity and carbonation efficiency compared to CO_2. This is due to the fact that NH_4HCO_3 provides a better source of CO_3^{2-} , compared with CO_2.

2. The experimental results show that carbonation efficiency exhibits two different behaviors with increasing temperature. Carbonation efficiency increases to a maximum value when the temperature is increased from 25 °C to 75 °C and then it gradually decreases when increasing temperature to 300 °C. A maximum carbonation efficiency of 53% and 98% is achieved using CO_2 and NH_4HCO_3, respectively.
3. The carbonation results show that all iron ions prior to carbonation stage are carbonated successfully, which results in an iron carbonation efficiency of 100% in all experiments.
4. High purity $CaCO_3$, as the main target of this study, is produced successfully. However, $CaCO_3$ purity is slightly higher when NH_4HCO_3 is used rather than CO_2. A maximum $CaCO_3$ purity of 92.57% and 99.05% is achieved using CO_2 and NH_4HCO_3, respectively.

Acknowledgement

The authors would like to appreciate the Department of Petroleum Engineering, Marvdasht Branch, Islamic Azad University, Marvdasht, Iran for the provision of the laboratory facilities necessary for completing this work. We would also like to thank Dr. Peter Dunning from University of Aberdeen for English proofreading of this manuscript.

References:

[1]. D. O. Metz B, de Coninck HC, Loos M, Meyer LA, "IPCC special report on carbon dioxide capture and storage. Prepared by working group III of the intergovernmental panel on climate change," ed. USA: Cambridge University Press, 2005.

[2]. S.J. Han, J.H. Wee. 2017. Carbon Dioxide Fixation by Combined Method of Physical Absorption and Carbonation in NaOH-Dissolved Methanol. Energy Fuels, Article ASAP, DOI: 10.1021/acs.energyfuels.6b02709.

[3]. S.P. Veetil, G. Mercier, J. Blais, E. Cecchi, S. Kentish. 2015. Magnetic separation of serpentinite mining residue as a precursor to mineral carbonation. International Journal of Mineral Processing. 140: 19-25.

[4]. E. R. Bobicki, Q. Liu, Z. Xu, and H. Zeng. 2012. Carbon capture and storage using alkaline industrial wastes. Progress in Energy and Combustion Science, 38: 302-320.

[5]. L.J. Kirwan, A. Hartshorn, J.B. McMonagle, L. Fleming, D. Funnell. 2013. Chemistry of bauxite residue neutralisation and aspects to implementation. International Journal of Mineral Processing. 119: 40-50.

[6]. S. Lavikko, O. Eklund. 2016. The significance of the serpentinite characteristics in mineral carbonation by "the ÅA Route". International Journal of Mineral Processing. 152: 7-15.

[7]. A. Hemmati, J. Shayegan, J. Bu, T.Y. Yeo, P. Sharratt. 2014. Process optimization for mineral carbonation in aqueous phase. International Journal of Mineral Processing. 130: 20-27.

[8]. H.-B. Duan, Y. Fan, and L. Zhu. 2013. What's the most cost-effective policy of CO_2 targeted reduction: An application of aggregated economic technological model with CCS?. Applied Energy, 112: 866-875.

[9]. T. Hosseini, C. Selomulya, N. Haque, L. Zhang. 2015. Investigating the Effect of the Mg^{2+}/Ca^{2+} Molar Ratio on the Carbonate Speciation during the Mild Mineral Carbonation Process at Atmospheric Pressure. Energy Fuels. 29 (11): 7483–7496.

[10]. J. Li, M. Hitch. 2017. Ultra-fine grinding and mechanical activation of mine waste rock using a planetary mill for mineral carbonation. International Journal of Mineral Processing. 158: 18-26.

[11]. S. Park, K. Song, C.W. Jeon. 2016. A study of mineral recovery from waste ashes at an incineration facility using the mineral carbonation method. International Journal of Mineral Processing. 155: 1-5.

[12]. E. Turianicová, P. Baláž, Ľ. Tuček, A. Zorkovská, V. Zeleňák, Z. Németh, A. Šatka, J. Kováč. 2013. A comparison of the reactivity of activated and non-activated olivine with CO_2. International Journal of Mineral Processing. 123: 73-77.

[13]. A. Azdarpour, M. Asadullah, E. Mohammadian, H. Hamidi, R. Junin, M. Afkhami Karaei. 2015. A Review on Carbon Dioxide Mineral Carbonation Through pH-swing Process. Chemical Engineering Journal, 279: 615–630.

[14]. A. Azdarpour, M. Asadullah, E. Mohammadian, R. Junin, H. Hamidi, M. Manan, A.R.M. Daud. 2015. Mineral carbonation of red gypsum via pH-swing process: Effect of CO_2 pressure on the efficiency and products characteristics. Chemical Engineering Journal, 264: 425–436.

[15]. W. Seifritz. 1990. CO_2 disposal by means of silicates. Nature, 345: 486.

[16]. G.L.A.F. Arce, T.G. Soares Neto, I. Avila, C.M.R. Luna, J.A. Carvalho Jr. 2017. Leaching optimization of mining wastes with lizardite and brucite contents for use in indirect mineral carbonation through the pH swing method. Journal of Cleaner Production, 141: 1324-1336.

[17]. S. Park, K. Song, C.W. Jeon. 2016. A study of mineral recovery from waste ashes at an incineration facility using the mineral carbonation method. International Journal of Mineral Processing, 155: 1-5.

[18]. A. Azdarpour, M. Asadullah, R. Junin, M. Manan, H. Hamidi, E. Mohammadian. 2014. Direct carbonation of red gypsum to produce solid carbonates. Fuel Processing Technology, 126: 429-434.

[19]. A. Azdarpour, M. Asadullah, R. Junin, E. Mohammadian, H. Hamidi, A. R. M. Daud, M. Manan. 2015. Extraction of calcium from red gypsum for calcium carbonate production. Fuel Processing Technology, 130: 12-19.

[20]. S.M. Pérez-Moreno, M.J. Gázquez, J.P. Bolívar. CO_2 sequestration by indirect carbonation of artificial gypsum generated in the manufacture of titanium dioxide pigments. Chemical Engineering Journal, 262: 737-746.

[21]. M.G. Lee, Y.N. Jang, K.W. Ryu, W. Kim, J.H. Bang. 2012. Mineral carbonation of flue gas desulfurization gypsum for CO_2 sequestration. Energy, 47: 370-377.

[22]. W. Huijgen, G. Witkamp, R. Comans. 2006. Mechanisms of aqueous wollastonite carbonation as a possible CO_2 sequestration process. Chem. Eng. Sci. 61: 4242–4251.

[23]. W. Huijgen, G. Witkamp, R. Comans. 2005. Mineral CO_2 sequestration by steel slag carbonation. Environ. Sci. Technol. 39: 9676–9682.

[24]. Z.Y. Chen, W.K. O'Connor, S.J. Gerdemann. 2006. Chemistry of aqueous mineral carbonation for carbon sequestration and explanation of experimental results. Environ. Prog. 25: 161–166.

[25]. L. Zhao, L. Sang, J. Chen, J. Ji, and H. H. Teng. 2010. Aqueous Carbonation of Natural Brucite: Relevance to CO_2 Sequestration. Environmental Science & Technology, 44: 406-411.

[26]. M. Dri, A. Sanna, and M. M. Maroto-Valer. 2013. Dissolution of steel slag and recycled concrete aggregate in ammonium bisulphate for CO_2 mineral carbonation. Fuel Processing Technology, 113: 114-122.

[27]. A. Sanna, X. Wang, A. Lacinska, M. Styles, T. Paulson, and M. M. Maroto-Valer. 2013. Enhancing Mg extraction from lizardite-rich serpentine for CO_2 mineral sequestration. Minerals Engineering, 49: 135-144.

[28]. A. Sanna, M. Dri, and M. Maroto-Valer. 2013. Carbon dioxide capture and storage by pH swing aqueous mineralisation using a mixture of ammonium salts and antigorite source. Fuel, 114: 153-161.

[29]. A. Sanna, A. Lacinska, M. Styles, and M. M. Maroto-Valer. 2014. Silicate rock dissolution by ammonium bisulphate for pH swing mineral CO_2 sequestration. Fuel Processing Technology, 120: 128-135.

[30]. R.M. Santos, J. Van Bouwel, E. Vandevelde, G. Mertens, J. Elsen, T. Van Gerven. 2013. Accelerated mineral carbonation of stainless steel slags for CO_2 storage and waste valorization: Effect of process parameters on geochemical properties. International Journal of Greenhouse Gas Control, 17: 32–45.

[31]. Y. Sun, M-S. Yao, J-P. Zhang, G. Yang. 2011. Indirect CO_2 mineral sequestration by steelmaking slag with NH_4Cl as leaching solution. Chemical Engineering Journal, 173: 437-445.

[32]. J. Zhang, R. Zhang, H. Geerlings, J. bi. 2012. Mg-Silicate Carbonation Based on an HCl- and NH_3 Recyclable Process: Effect of Carbonation Temperature. Chem. Eng. Technol. 35: 525–531.

[33]. W. Wang, M. Hu, Y. Zheng, P. Wang, C. Ma. 2011. CO_2 fixation in Ca^{2+}-/Mg^{2+}-rich aqueous solutions through enhanced carbonate precipitation. Industrial & Engineering Chemistry Research, 50: 8333–8339.

[34]. L. He, D. Yu, W. Lv, J. Wu, M. Xu. 2013. A Novel Method for CO_2 Sequestration via Indirect Carbonation of Coal Fly Ash. Ind. Eng. Chem. Res., 52: 15138-15145.

[35]. S. Gopi, V.K. Subramanian, K. Palanisamy. 2013. Aragonite-calcite-vaterite: A temperature influenced sequential polymorphic transformation of $CaCO_3$ in the presence of DTPA. Materials Research Bulletin, 48: 1906–1912.

[36]. Ö, Cizer, K. Van Balen, J. Elsen, D. Van Gemert. 2012. Real-time investigation of reaction rate and mineral phase modifications of lime carbonation. Construction and Building Materials, 35: 741–751.